Elastic, inelastic, and one-nucleon transfer processes in ^{48}Ca + ^{64}Ni

D. Montanari,[1,*] S. Leoni,[1,2,†] L. Corradi,[3] G. Pollarolo,[4] G. Benzoni,[2] N. Blasi,[2] S. Bottoni,[1] A. Bracco,[1,2] F. Camera,[1,2] A. Corsi,[1,2] F. C. L. Crespi,[1,2] B. Million,[2] R. Nicolini,[1,2] O. Wieland,[2] G. de Angelis,[3] F. Della Vedova,[3] E. Fioretto,[3] A. Gadea,[5] B. Guiot,[3] D. Mengoni,[3,6] D. R. Napoli,[3] R. Orlandi,[3,‡] F. Recchia,[7] A. M. Stefanini,[3] R. P. Singh,[3] J. J. Valiente-Dobon,[3] D. Bazzacco,[8] E. Farnea,[8] S. M. Lenzi,[7,8] S. Lunardi,[7,8] G. Montagnoli,[7,8] F. Scarlassara,[7,8] C. Ur,[8] G. Lo Bianco,[9] A. Zucchiatti,[10] S. Szilner,[11] M. Kmiecik,[12] A. Maj,[12] and W. Meczynski[12]

[1]*Dipartimento di Fisica, University of Milano, Milano, Italy*
[2]*INFN, Sezione di Milano, Milano, Italy*
[3]*Laboratori Nazionali di Legnaro, Padova, Italy*
[4]*Dipartimento di Fisica Teorica, University of Torino and INFN, Sezione di Torino, Italy*
[5]*CSIC-IFIC, Valencia, Spain*
[6]*University of the West of Scotland, Paisley, United Kingdom*
[7]*Dipartimento di Fisica, University of Padova, Padova, Italy*
[8]*INFN, Sezione di Padova, Padova, Italy*
[9]*University of Camerino and INFN, Sezione di Perugia, Italy*
[10]*INFN, Sezione di Genova, Genova, Italy*
[11]*Ruđer Bošković Institute, Zagreb, Croatia*
[12]*The Niewodniczanski Institute of Nuclear Physics, Polish Academy of Sciences, Krakow, Poland*

(Received 20 July 2011; published 17 November 2011)

Elastic, inelastic, and one-nucleon transfer channels in the ^{48}Ca + ^{64}Ni reaction have been measured at ≈6 MeV/nucleon with the PRISMA-CLARA setup, at Legnaro National Laboratory, consisting of the coupling of a large solid angle magnetic spectrometer with a germanium array. By trajectory reconstruction the reaction products have been fully identified in mass, nuclear charge, and kinetic energy, while coincident γ spectra of binary partners have been constructed after Doppler correction. Absolute differential cross sections have been extracted for the inelastic excitation and one-nucleon transfer, also for specific excited states. The data are in good agreement with semiclassical calculations and distorted wave Born approximation predictions. The work outlines an experimental method which can become valuable to extract structural information from heavy-ion reaction studies.

DOI: 10.1103/PhysRevC.84.054613 PACS number(s): 25.70.Bc, 25.70.Hi, 24.10.Eq, 27.40.+z

I. INTRODUCTION

Transfer reactions have always been of great importance in the study of nuclear structure and nuclear reaction dynamics. In the past, transfer reactions with light ions have provided detailed information on the nuclear shell model and on particle-particle correlations [1]. Later on, transfer reactions with heavy ions became important for a comprehensive understanding of complex reaction mechanisms involving quasielastic, deep-inelastic, and fusion regimes [2,3]. In more recent years, multinucleon transfer reactions have been shown to be a powerful tool for the production of nuclei far from stability and for the study of their nuclear dynamical [4] and nuclear structure [5] properties.

Experimentally, a key instrument in multinucleon reaction studies is a large acceptance magnetic spectrometer coupled to a high efficiency and high resolution multidetector array for γ spectroscopy, based on Ge detectors. Such a combination turned out to be very successful in studies linking nuclear structure and reaction mechanism, for nuclei which can be populated with competitive rates compared with other production methods, especially for the investigation of selected excited states [6,7].

In this work we made a study of the binary reaction ^{48}Ca + ^{64}Ni, at a beam energy of approximately 6 MeV/nucleon. Making use of the PRISMA-CLARA setup [8,9], at the INFN National Laboratory of Legnaro (Italy), we performed coincidences between the ions, fully identified with the PRISMA magnetic spectrometer, and their associated γ transitions, measured with the CLARA Ge array. The analysis concentrates on the dynamics of the reaction, outlining an experimental procedure which can be considered as a first step for future possible applications oriented to the extraction of structural information (for recent results from γ-spectroscopy studies see Ref. [10]).

We present a comprehensive analysis on elastic, inelastic, and one neutron transfer processes. By combining the information provided by both PRISMA and CLARA, we extracted the differential cross sections for elastic scattering and those associated to the population of the first excited states of ^{48}Ca and ^{64}Ni. In the ^{48}Ca + ^{64}Ni system, optimum Q-value arguments favor, besides the pickup of neutrons and stripping of protons, the stripping of neutrons and pickup of protons, therefore we could make a broad-range comparison between data and model calculations. Also for transfer channels, by

*Present address: University of Padova, Padova, Italy.
†silvia.leoni@mi.infn.it
‡Present address: IEM-CSIC, Madrid, Spain.

combining data collected with these particle and γ-ray spectrometers, we could extract cross sections for specific nuclear states. Experimental data for elastic, inelastic, and transfer channels, have been compared to theoretical predictions either based on the semiclassical GRAZING model for colliding heavy ions [11], or on distorted wave Born approximation calculations performed by the code PTOLEMY [12]. The results show that the new method of analysis may potentially become very valuable for future investigations of heavy-ion transfer reactions, also in the case of radioactive heavy-ion beams, providing complementary information to transfer reactions with light targets. A first example in this type of studies with a radioactive ^{24}Ne beam is presented in Ref. [13]. The work shows that, with setups of comparable efficiencies, this analysis method can be applied down to a beam intensity of the order of 10^5.

The paper is organized as follows. In Sec. II we briefly describe the experimental setup, while in Sec. III we discuss the procedure adopted for the identification of the reaction products in the magnetic spectrometer, outlining also how its response function was evaluated. The study of the elastic, inelastic, and one-particle transfer data is presented in Secs. IV and V. Conclusions are given in Sec. VI.

II. THE EXPERIMENTAL SETUP

The experiment has been performed at Laboratori Nazionali di Legnaro of INFN, using the PRISMA-CLARA setup [9]. The ^{48}Ca beam at 282 MeV of bombarding energy was provided by the Tandem-ALPI complex, with an average intensity of 1 pnA. The beam impinged on a ^{64}Ni target, 0.98 mg/cm^2 thick, placed at 45° with respect to the beam direction. The energy loss of the projectile in the middle of the target was estimated to be 7.9 MeV. Projectile-like products have been selected with the magnetic spectrometer PRISMA placed at $\theta_{\rm lab} = 20°$, the grazing angle for this reaction.

The configuration of PRISMA and its detector system have been described in details in Refs. [14–16], here we only recall its main characteristics. PRISMA consists of a system of one quadrupole and one dipole magnet, with a solid angle of ∼80 msr (corresponding to ±6° in θ and ±11° in ϕ), a momentum acceptance $\Delta p/p = \pm 10\%$ and a dispersion of ∼4 cm per percent in momentum.

Due to the large acceptance and the minimum number of magnetic elements PRISMA does not have a well-defined focus and the mass and charge identification are based on the reconstruction of the ion trajectories [16]. This is obtained with a detection system providing information on two-dimensional positions at the entrance and the exit of the spectrometer, time-of-flight (TOF), and energy loss. The entrance detector is based on a two-dimensional position sensitive microchannel plate (MCP), giving a start signal for TOF (with sub-nanosecond resolution) and X, Y signals (with 1 mm resolutions) [14]. The detector system at the focal plane consists of an array of parallel plates of multiwire-type (MWPPAC), providing a stop signal for TOF and X, Y position signals (with 1 mm resolutions). It is followed by an multianode ionization chamber (IC), giving ΔE and total energy E signals [15]. The pressure of the gas filling the IC (CH_4 in the present experiment) is adjusted in order to provide the optimum nuclear charge resolution.

The γ-ray array CLARA consisted of 23 Hp-Ge clover-type detectors placed to form a 2π configuration close to the target position and opposite to PRISMA [9]. Each clover detector is composed of four crystals mounted in a single cryostat and surrounded by an anti-Compton shield, ensuring a peak-to-total ratio of ∼50%. The total photopeak efficiency of CLARA is of the order of 3% for $E_\gamma = 1.33$ MeV. The intrinsic energy resolution of the Ge array is ∼3 keV for the transition at 1.3 MeV of a ^{60}Co source, while a FWHM of up to ∼10 keV is obtained for gamma rays released by projectile-like ions at 10% the speed of light (as typically measured in the ^{48}Ca + ^{64}Ni experiment).

III. ANALYSIS OF THE PRISMA DATA

The identification of the reaction products in PRISMA is based upon the reconstruction of the trajectories of the ions, on an event-by-event basis. The trajectories are reconstructed through the geometrical and timing information provided by PRISMA and by applying the equation of motion of a charged particle in the quadrupole and dipole magnetic fields [16,17]. To obtain a fast algorithm for the off-line sorting phase of the data, the trajectory is assumed to be planar. Under this assumption the trajectories are uniquely defined by only two parameters: the bending radius ρ in the dipole and the ratio of the quadrupole and dipole magnetic fields. The effects of the fringing fields are neglected. As a consequence, the bending radius ρ is the only parameter to be determined. This has been checked with a simulation of the transport of the ions through the spectrometer by using the actual fields and a Monte Carlo method to reproduce the distribution of the reaction products [16].

The assignment of the atomic number Z is obtained by using the energy loss ΔE and the total kinetic energy E of the ions as provided by the ionization chamber. The correlation matrix ΔE-E obtained for the ^{48}Ca + ^{64}Ni system is shown in the top panel of Fig. 1: each ridge corresponds to a different atomic number Z, the most intense one being associated to the Z of Ca isotopes and setting a reference for all other Z's. Notice that the ΔE-E matrix, at this measured bombarding energy and angle, displays distinct global event distributions with average ΔE centroids around channels 2500 and 1500, which are associated with quasielastic components and to components with large energy loss, respectively.

The reconstruction of the mass number A, is based on the relation $A/q \propto B\rho/v$ which follows from the Lorentz equation, here v is the velocity of the ion, which is given by $v = L/\mathrm{TOF}$, being L the length of the trajectory.

Due to the existence of several atomic charge states q, different A/q values are obtained for each Z and a selection of the single charge states is needed to construct the mass spectra. From the Lorentz equation it is possible to derive the proportionality $E \propto q\rho\beta$, where E is the total kinetic energy and $\beta = v/c$ the velocity. Therefore, a two-dimensional plot of E versus ρv allows to select the atomic charge state (as shown

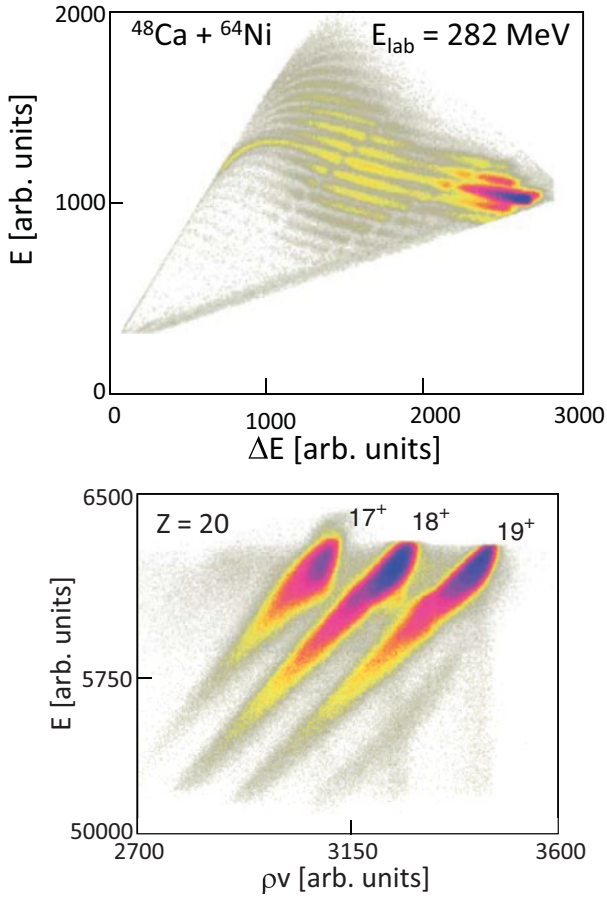

FIG. 1. (Color online) Top: ΔE-E spectrum of the reaction ^{48}Ca + ^{64}Ni, as measured by the ionization chamber of PRISMA. The most intense distribution is associated to $Z = 20$. The diagonal line is a trivial effect due to detector thresholds. Bottom: E versus ρv spectrum showing the atomic charge state distribution for $Z = 20$. The distribution is peaked at $q = 18^+$, with less than 7% intensity going into $q = 16^+$ and 20^+ (cf. Ref. [16]).

in the bottom part of Fig. 1 for $Z = 20$), and to finally construct the mass spectra for each isotopic chain. Figure 2 presents the mass spectra for the isotopic chains up to the $-2p$ (proton stripping) and $+2p$ (proton pickup) range, as measured in the experiment. The spectra are plotted, for each nuclear charge, as function of the number of transferred neutrons (ΔN).

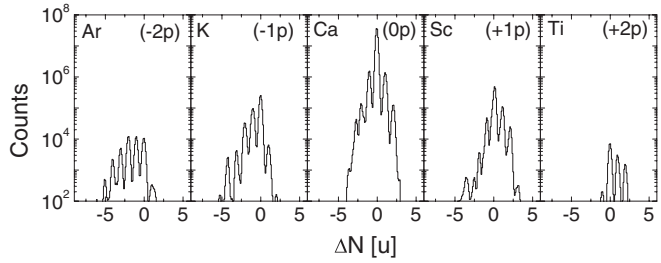

FIG. 2. Mass spectra of the most intense isotopic chains produced in the ^{48}Ca + ^{64}Ni experiment, plotted as function of the number of transferred neutrons (ΔN).

For pure neutron transfers one sees a quite symmetric yield distribution between the pickup and stripping, with the $+1n$ and $+2n$ channels comparable to the $-1n$ and $-2n$ ones, respectively. This finding is consistent with what one expects on the basis of optimum Q-value arguments. The lack of the $+3n$ channel, corresponding to ^{51}Ca, suggests that neutron evaporation plays an important role [18,19], especially for (primary) produced nuclei with low binding energies (we here remind that we detect secondary fragments). For pure proton transfers one notices that the ratio of $+1p$ and $+2p$ channels is, within a factor $\sim$2, comparable with that of $-1p$ and $-2p$ ones, also in rough agreement with optimum Q values. On the other hand, in the proton stripping sector a shift toward lighter masses is clearly seen indicating that the mechanism populating these nuclei is quite different from the one on the proton pick-up sector. While in the proton pick-up sector the (not shown) total kinetic energy loss (TKEL) is concentrated in a narrow energy interval close to the ground state Q values, in the proton stripping sector the TKEL is much larger indicating that more complex mechanisms (like deep-inelastic, we are at twice the Coulomb barrier) populate these masses. Also the evaporation of neutrons will act very differently in the two sectors favoring lighter masses for the proton stripping one.

To obtain the cross sections, the transmission of the ions through the magnetic spectrometer was carefully evaluated. Following the procedure described in Ref. [16] we started from a uniform, spatial and kinetic energy, distribution of the incoming particles, here ^{48}Ca. The response function of PRISMA is then calculated for each value of energy and angle, as the ratio of the transported events over the initial ones. This function $f(E_K, \theta_{\rm lab})$ has been constructed by using five million events and by adopting a step of 0.1 MeV for the energy and of 0.2° for the scattering angle. The statistical fluctuations of the transport function, needed to estimate the induced errors, have been estimated by adopting a smoothing procedure. The original function has been smoothed four times, using two Gaussian averaging and two moving average methods, each within square boxes of three and five channels side. The response function used to correct experimental data has been constructed by making the average, for each E_K and $\theta_{\rm lab}$ value, of the original $f(E_K, \theta_{\rm lab})$ function and the four smoothed ones. The errors are found to be of the order of 20%. In the following analysis, the error bars on the experimental points account for both statistical errors, taken as the standard deviation, and the errors on the transport function.

IV. ELASTIC AND INELASTIC SCATTERING

The starting point in the analysis of cross sections is the study of the elastic scattering. In the case of heavy-ion collisions the extraction of true elastic scattering is not easy. One deals with many open channels which can hardly be separated since the available experimental techniques unavoidably have a finite energy resolution. Here, to estimate the intensity of the elastic channel we adopt the procedure described in Ref. [17].

For each $\theta_{\rm lab}$ two total kinetic energy loss spectra have been constructed, the first built with the only requirement

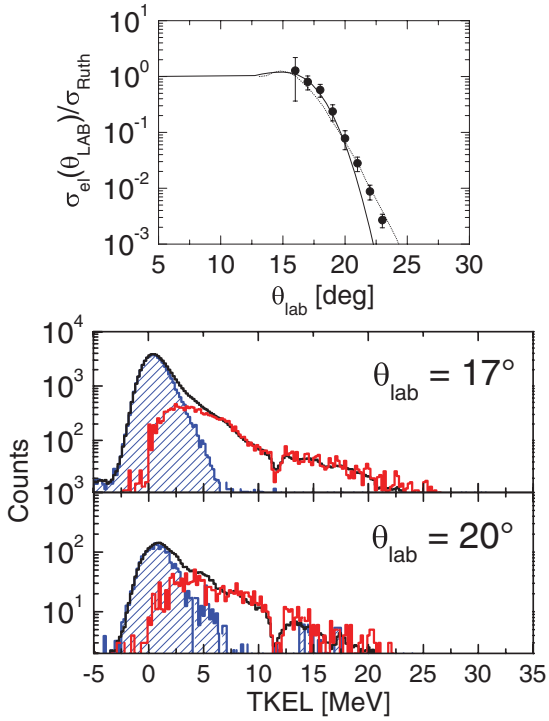

FIG. 3. (Color online) Top: Ratio between the elastic cross section σ_{el} and the Rutherford cross section σ_{Ruth}. Full dots represent the experimental values normalized at $\theta_{\text{lab}} = 17^{\circ}$, solid and thin lines are the theoretical calculation by the GRAZING model [11] and by the code PTOLEMY [12], respectively. Bottom: TKEL spectra for ^{48}Ca ions at the indicated angles. The black spectra are obtained with the only request of a ^{48}Ca ion detected in PRISMA, while the red ones are constructed with the additional request of a γ ray in coincidence in the Ge array. The shaded histograms are the difference spectra.

of detecting a ^{48}Ca ion in PRISMA (black lines in the bottom part of Fig. 3), the second obtained requiring an additional coincidence with γ rays measured by CLARA (red lines). These two spectra are normalized in the (inelastic) tail region (above ≈6 MeV) and finally the difference spectrum is obtained by subtraction (blue shaded peaks). The counts in the peak, at the most forward angles, are considered to be mainly due to pure elastic scattering. The elastic peak is centered at TKEL ≈0 and its width is ≈2.5 MeV, consistent with the experimental energy resolution. The extracted cross sections, as a function of the scattering angle, are shown in the top part of Fig. 3 as ratio to the Rutherford cross section. In constructing this plot we assumed that at the most forward angle the elastic cross section is well approximated by the Rutherford scattering, thus obtaining the absolute normalization factor (in mb/sr) for all other angles and for all other reaction channels.

Of course this normalization procedure is correct only if we are really in the Rutherford regime at the forward angles, from the behavior of the data we cannot be that sure since the data display a monotonic decay all over the measured angular range. In the present PRISMA settings the energy of the elastic scattering at 16° corresponds to a momentum at the limit of the acceptance of the magnetic spectrometer, which explains the rather large error bar reported at this angle. To have, at least a partial confirmation that our procedure is valid we calculated the elastic angular distribution by using the semiclassical coupled-channels model GRAZING [11]. This model is able to include the depopulation of the elastic scattering via the Coulomb excitation of the low-lying states of target and projectile, to estimate the contribution coming from the nuclear part of the form factor and the contribution coming from the transfer reactions. The result of such a calculation is shown with the solid line in the top part of the figure. Since in this calculation the relative motion is treated classically the model is underpredicting the cross section at backward angle. By using the same real potential as in GRAZING ($V_0 = -68.8$ MeV, $a = 0.67$ fm, and $r_0 = 1.18$ fm) and for the imaginary part the one estimated by the same model ($W_0 = -50$ MeV, $a = 0.67$ fm, and $r_0 = 1.18$ fm) we have performed an optical model calculation by using the code PTOLEMY. The result of such a calculation is shown with a thin line in the same figure.

We are aware that the adopted experimental procedure presents some limitation, especially at very backward angles, where the TKEL spectra are strongly affected by inelastic processes. Nevertheless, the overall reasonable agreement between the theoretical curves and the experimental data, up to a ratio $\sigma_{el}/\sigma_{\text{Ruth}} \approx 0.1$, gives us confidence that the extracted experimental yield at the most forward angles is due to pure elastic scattering and that we are in the Coulomb scattering regime. Therefore, the conversion factor $C = 1$ mb/sr = 2828 counts, here obtained, may be kept as a reference for the analysis that will follow.

To extract the angular distribution for the inelastic scattering to the low-lying states of target and projectile we make use of the TKEL spectra measured in coincidence with γ transitions detected by the CLARA array. In panels (a) and (b) of Fig. 4 are shown, for illustrative purposes, the correlation matrices E_γ versus TKEL. Here, to have more statistics, we integrated over the whole measured angular range, for the projectile and the target. To obtain the correct energy of the γ's, Doppler correction had to be applied. Projecting these correlation functions on the E_γ axis one obtains the γ spectra for ^{48}Ca (c) and ^{64}Ni (d), respectively.

The two-dimensional distributions of panels (a) and (b), in correspondence with the γ decay from specific nuclear states, show stripes extending to rather high TKEL values. For the ^{48}Ca are clearly visible the stripes corresponding to the $2^+ \rightarrow 0^+$ transitions at $E_\gamma = 3832$ keV and to the transition at 672 keV that is feeding the 2^+ state. For the ^{64}Ni are visible the $2^+ \rightarrow 0^+$ transition at 1346 keV and the one at 930 keV that is also feeding the previous one. By setting gates on the γ peaks, the TKEL spectra in coincidence with the $2^+ \rightarrow 0^+$ (blue histograms) and corresponding feeding (red histograms) transitions are obtained from the two-dimensional matrices, as shown in panels (e) and (f). The difference spectra (shaded histograms) are found to be well reproduced by Gaussian fits largely dominated by one component, with a centroid consistent with the reaction Q value of the 2^+ states (i.e., −3.8 and −1.3 MeV for the ^{48}Ca and ^{64}Ni cases, respectively). This indicates that the intensity of the peaks in the subtracted TKEL spectra can be attributed to the direct

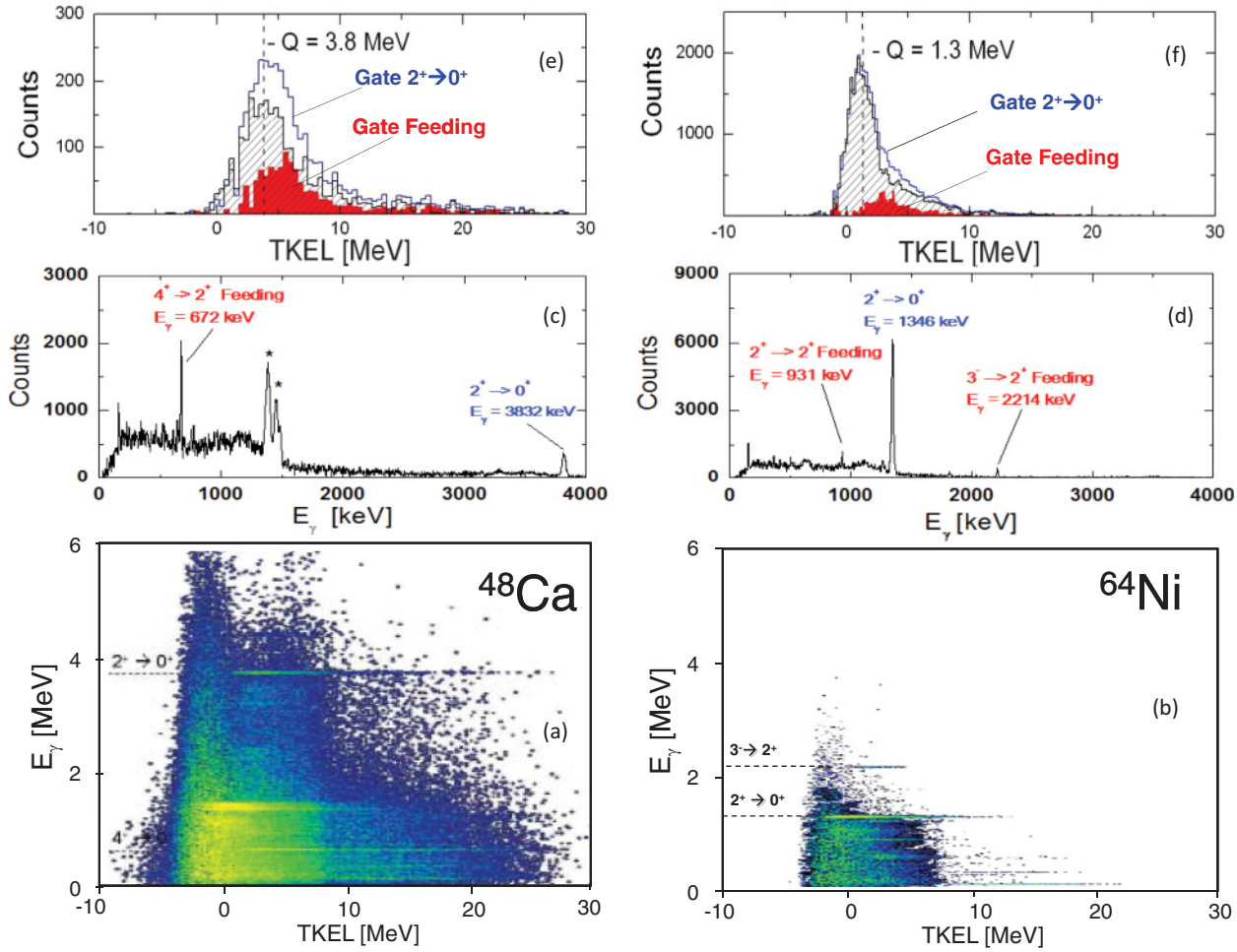

FIG. 4. (Color online) (a) and (b) Correlation matrices E_γ versus TKEL for ^{48}Ca and ^{64}Ni, integrated over the entire angular range of PRISMA. Projection of the E_γ axis are shown in (c) and (d). Contaminant lines from the partner nucleus are marked by stars. TKEL spectra gated by specific γ transitions of ^{48}Ca and ^{64}Ni are shown in (e) and (f), respectively. The blue histograms are in coincidence with the $2^+ \rightarrow 0^+$ transitions, the filled red ones with the feeding transitions. The spectra are background subtracted by setting narrow gates in the 2D matrices, beside the γ peaks. The shaded histograms are the difference spectra between the $2^+ \rightarrow 0^+$ and the corresponding feeding distributions.

population of the 2^+ states in the inelastic scattering process. We note that in the case of ^{64}Ni a tail is observed at high energy in the TKEL spectrum, with a centroid around 4 MeV and an intensity increasing at larger angles. This comes from the feeding from several unresolved states in the 3 to 5 MeV excitation energy region [20]. On the contrary, in the case of ^{48}Ca, the 2^+ state is reported to be fed from fewer unresolved states from an higher excitation energy region (above 5 MeV), not so well populated in this reaction.

The subtraction procedure just outlined has been performed for each angle $\theta_{\rm lab}$ covered by the acceptance of the PRISMA spectrometer ($15^\circ \leqslant \theta_{\rm lab} \leqslant 25^\circ$). In this way we constructed the corresponding angular distributions for the 2^+ states of both ^{48}Ca and ^{64}Ni, with absolute values deduced from the normalization procedure previously discussed for the elastic scattering. The results are shown as open symbols in Fig. 5. To give further confidence on the adopted procedure, we independently extracted the direct population of the first excited states of projectile and target without passing through the TKEL distributions, i.e., from the intensity of the $2^+ \rightarrow 0^+ \gamma$ transitions, after subtracting the feeding contribution from the $4^+ \rightarrow 2^+$ decay and taking into account the γ efficiency of the CLARA array. The results are displayed in the same figure as full symbols, which turn out to be very close to the full ones. The solid lines are the theoretical predictions based on the distorted wave Born approximation (DWBA) model, calculated with the code PTOLEMY [12]. For the matrix elements we used the macroscopic model for the nuclear part of the form factor and the exact expression for the Coulomb part. The deformation parameters β_λ are kept the same for the nuclear and Coulomb parts, in particular we have used for the 2^+ states in ^{48}Ca the value $\beta_2{}^+ = 0.1$ and in ^{64}Ni the value $\beta_2{}^+ = 0.18$ that are in good agreement with the adopted values.

V. TRANSFER REACTION CHANNELS

The ^{48}Ca nucleus is the most neutron-rich among stable Ca isotopes. Because of this, nuclear collisions with this projectile

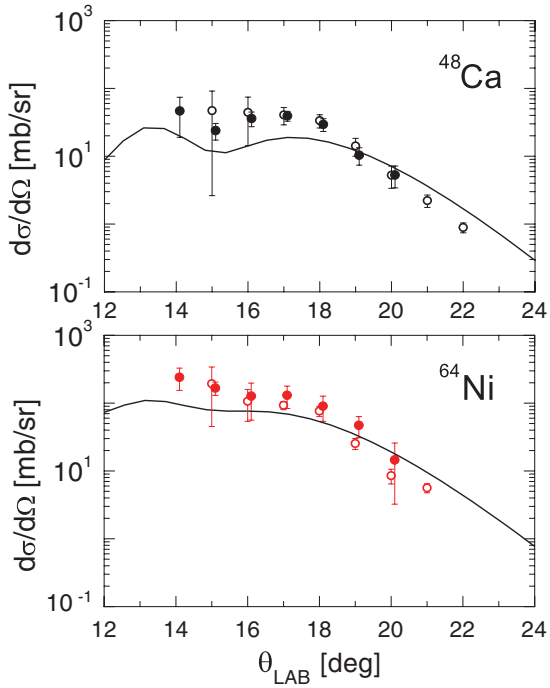

FIG. 5. (Color online) Angular distributions of the 2^+ states of ^{48}Ca (top panel) and ^{64}Ni (bottom panel). Empty (full) symbols refer to the analysis on TKEL (γ) spectra. The solid lines represents the theoretical values obtained by DWBA calculations with the code PTOLEMY [12], with parameters given in the text.

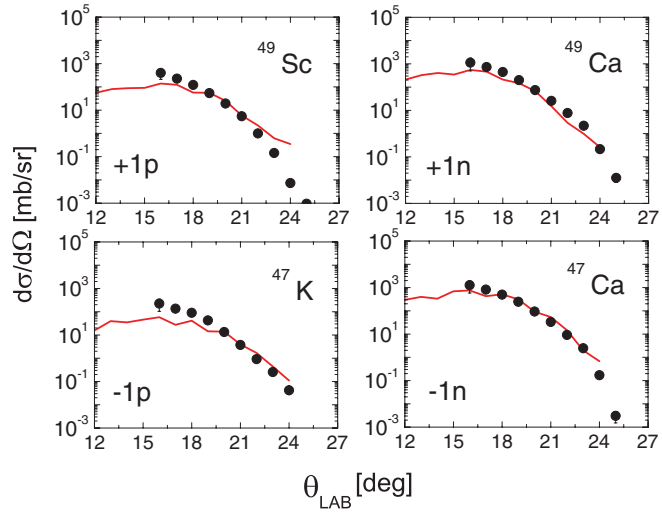

FIG. 6. (Color online) Angular distributions for the $\pm 1n$ and $\pm 1p$ transfer channels. The experimental data are shown by symbols while the solid lines give the theoretical predictions from the semiclassical model GRAZING [11].

are very rich in the sense that in the reaction it is possible to populate at once not only the usual neutron pick-up and proton stripping channels but also to reach a sizable population for the neutron-stripping and proton pick-up channels. This fact is easily understood from simple Q-value consideration, since the optimum Q value of a reaction is essentially dominated by the properties of the lighter projectile. To have the full family of transfer reactions is very appealing from a theoretical point of view since this allows to have, at least for the one nucleon transfer reactions, a comparison of the full parametrization of the matrix elements governing the transfer process. Here we recall that in the semiclassical code GRAZING the one-nucleon transfer channels constitute the building blocks over which are built the estimations for multinucleon transfer channels.

In Fig. 6 we show the experimental angular distributions of all inclusive one-nucleon transfer channels (^{47}K, ^{49}Sc, ^{47}Ca, and ^{49}Ca), obtained by integrating, angle by angle, the TKEL spectra measured in PRISMA. The data are shown together with the results of the code GRAZING. We remind the reader that in this model the basic degrees of freedom consist of single particle and surface vibrations around the spherical equilibrium shape, including the lowest 2^+ and 3^- states and the associated giant resonances. The exchange of nucleons is governed by microscopic form factors taking into account the single particle properties of the two interacting ions and an average single particle level density. One sees how the experimental angular distributions are quite well reproduced by calculations, both in shape and in absolute values, providing a global agreement between data and theory, although some discrepancies can be noticed at the most forward angles.

In this γ-particle coincidence experiment we have the chance to be more specific in our analysis of transfer data, we may be able to infer the population of single particle states. In the following we will try to do this by focusing solely on the neutron pick-up ($+1n$) channel since for this channel we have enough statistics to be able to use the technique explained above for the elastic and inelastic channels.

In Fig. 7(a) we show the two-dimensional correlation matrix E_γ (Doppler corrected for ^{49}Ca) versus TKEL, corresponding to the detection of ^{49}Ca ions in the spectrometer. The matrix shows stripes parallel to the TKEL axis in coincidence with the γ decay from excited states of ^{49}Ca, as indicated in the projection on the E_γ axis [panel (b)]. Panel (c) shows, by black and red histograms, the TKEL spectra without and with coincidence with a γ, respectively, normalized in the high-energy tail region (above 10 MeV). The resulting difference spectrum (shaded histogram) is found to be dominated by a Gaussian component with a centroid at ≈4.5 MeV. The width of this transfer data is larger then the one obtained for the elastic and inelastic channels and it is compatible with reactions that leave ^{49}Ca in its ground state and involve the ground and the first excited states of ^{63}Ni, up to an excitation energy of ∼1.3 MeV (see below). By adopting this procedure in steps of one degree over the PRISMA angular acceptance we obtained the angular distribution shown by symbols in Fig. 8(a).

The interpretation of the experimental angular distribution has been based on calculations performed in the DWBA approximation

$$\frac{d\sigma}{d\Omega} = S_{\mathrm{Ca}} \times S_{\mathrm{Ni}} \times \left(\frac{d\sigma}{d\Omega}\right)_{\mathrm{DWBA}}, \qquad (1)$$

where S_{Ca} and S_{Ni} are the spectroscopic factors of the considered single particle states of the two nuclei, given in

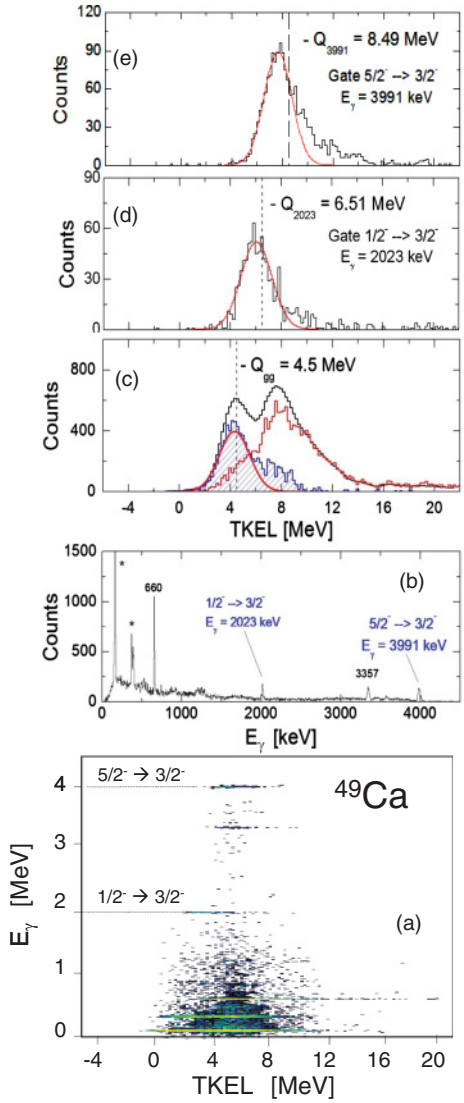

FIG. 7. (Color online) (a) Correlation matrix E_γ versus TKEL for ^{49}Ca, integrated over the entire angular range of PRISMA. The projection on the E_γ axis is shown in (b). The energy of the strongest γ transitions of ^{49}Ca are indicated by labels, while contaminant lines from the partner nucleus are marked by stars. (c) gives the TKEL spectra measured by PRISMA (black histogram) and with the requirement of a γ coincidence in the Ge array (red curve). The difference spectrum is shown by the shaded distribution, with superposed the Gaussian fit of the main component (with centroid and FWHM equal to 4.3 and 2.5 MeV). (d) and (e) give the TKEL spectra gated by the 2023 and 3991 keV γ transitions of ^{49}Ca, with the corresponding Gaussian fit (red line).

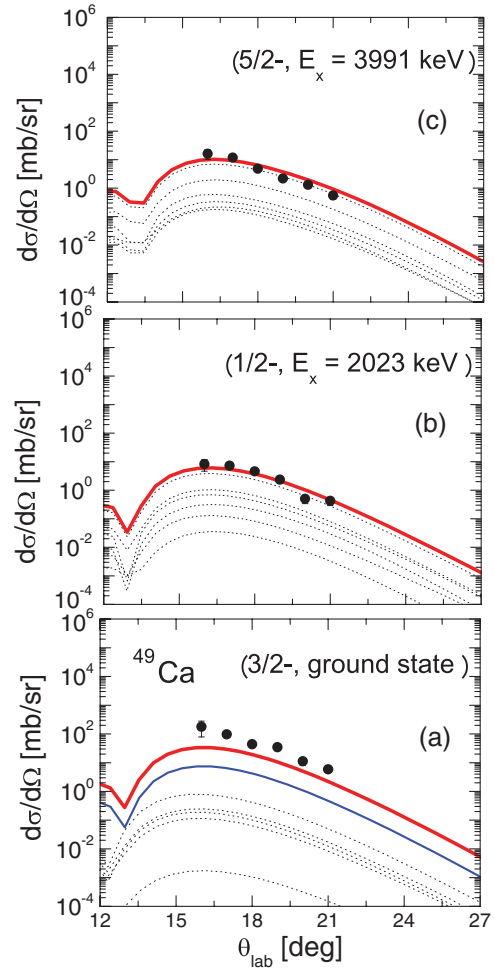

FIG. 8. (Color online) Angular distributions of transfer reactions leading to the population of ^{49}Ca ions close to the ground state (a) and to the excited states at 2023 and 3991 keV (b) and (c). The experimental data are given by symbols, theoretical DWBA predictions by red lines. The calculations are obtained by summing the components given by dotted lines, corresponding to the excitation of the partner nucleus ^{63}Ni to states within 2 MeV of excitation energy. In (a) the thin solid, blue line corresponds to the transfer cross section with ^{63}Ni in the ground state.

Table I [20]. The DWBA calculations have been performed with the code PTOLEMY using for the optical potential the parameters determined for the elastic scattering (see above). The transfer matrix elements have been constructed, in the full recoil approximation, by using for the volume part of shell model potential the standard Woods-Saxon shape with $r_0 = 1.2$ fm and $a = 0.65$ fm for the Ca and $r_0 = 1.28$ fm and $a = 0.76$ for the Ni. The spin orbit was kept to be proportional to the r derivative of the volume one for the Ca nucleus ($V_{SO} = 7$ MeV), while one has to use a somewhat different parametrization for the Ni nucleus ($r_{SO} = 1.09$ fm, $a_{SO} = 0.6$ fm) with a normalization of $V_{SO} = 6$ MeV. The depth of the volume part of the potential has been adjusted to provide the correct binding energies that for the different single particle states included in the calculation are reported in Table I.

Of course, the energy resolution of ∼2.5 MeV and the lack of γ-γ coincidences (due to limited γ detection efficiency) do not allow to disentangle contributions from the excitation of low-energy states of the partner nucleus ^{63}Ni. The presence of these states is indeed suggested by the width and tail visible in the TKEL spectrum [blue histogram in Fig. 7(c)].

Thus, for ^{63}Ni, in addition to the contribution given by the ground state (obtained creating a quasihole in the $2p_{1/2}$ state), we have summed contributions coming from excited states

TABLE I. Spectroscopic factors for the lowest single particle states of ^{49}Ca and ^{63}Ni [20].

	Spin [$\hbar$]	State	Energy [keV]	S
^{49}Ca	$3/2^-$	$p_{3/2}$	0	0.84
	$1/2^-$	$p_{1/2}$	2021	0.91
	$5/2^-$	$f_{5/2}$	3991	0.84
^{63}Ni	$1/2^-$	$p_{1/2}$	0	0.235
	$5/2^-$	$f_{5/2}$	87	0.572
	$3/2^-$	$p_{3/2}$	156	0.605
	$3/2^-$	$p_{3/2}$	518	0.205
	$1/2^-$	$p_{1/2}$	1002	0.260
	$9/2^+$	$g_{9/2}$	1294	0.082

lying within 2.5 MeV around the Fermi surface. These states correspond to single particle excitations in the $f_{5/2}$, $p_{3/2}$, $p_{1/2}$, and $g_{9/2}$ states, as shown in Fig. 9.

In panel (a) of Fig. 8 we show the theoretical angular distributions thus obtained, the blue line is the cross section corresponding to ^{63}Ni in the ground state and the thick red line is the sum of all the partial contributions (dotted and thin solid lines). Here the dominant contribution is given by the excitation of ^{63}Ni into the lowest $p_{3/2}$ state.

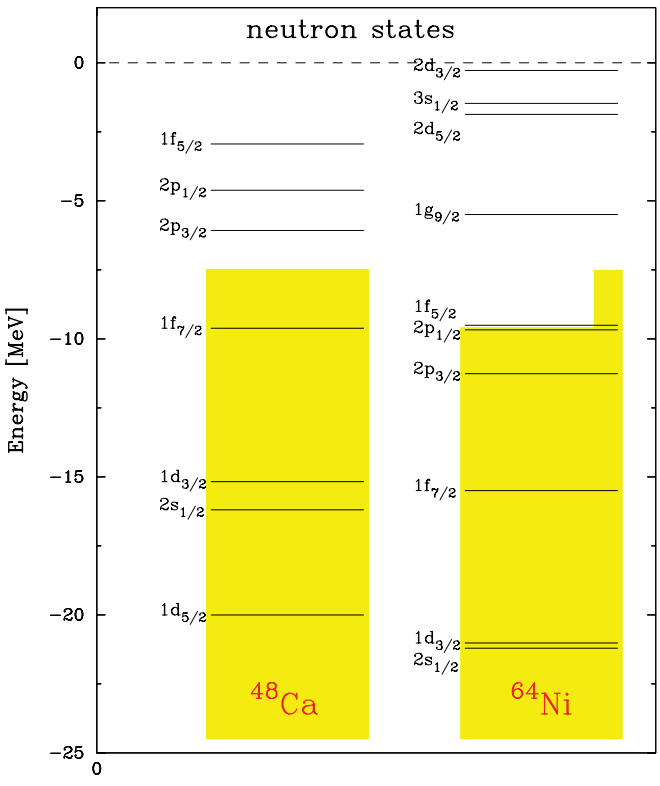

FIG. 9. (Color online) Single particle level scheme of the neutron states for ^{48}Ca and ^{64}Ni. The yellow areas correspond to the occupied levels below the Fermi surface, which in the case of ^{64}Ni is diffused due to the superfluidity of the nucleus.

The procedure adopted for the angular distribution of transitions leading to the ground states of ^{49}Ca may be generalized also to get the angular distributions of selected excited states of ^{49}Ca. This has been done by setting gates on the 2023 keV and 3991 keV transitions seen in Fig. 7, and which correspond to the de-excitation of the $1/2^-$ and $5/2^-$ single particle states of ^{49}Ca. In these cases no feeding from higher excitation energy regions of the spectrum has been observed, therefore we subtracted contributions only from the background by setting narrow gates on both sides of the γ peak of interest.

In panels (d) and (e) of Fig. 7 the result of the analysis are shown: in both cases a defined peak is found in the TKEL spectra in coincidence with the γ decay from the specific state, with a centroid close to the expected Q value for the direct transfer to that energy level, compatible with the energy resolution of the spectrometer. The corresponding experimental angular distributions for transfer reactions to the excited states at 2023 and 3991 keV of ^{49}Ca are shown by symbols in panels (b) and (c) of Fig. 8. The experimental data have been compared in both cases to DWBA predictions by the PTOLEMY code, calculated following Eq. (1), including, also in this case, contributions from the partner nucleus ^{63}Ni within 2.5 MeV of excitation energy (dotted and thin solid lines in the figure). Similarly to the ground state analysis of panel (a), reasonable agreement is obtained between data and theory, being the excitation of ^{63}Ni into the lowest $p_{3/2}$ state the dominant contribution to the cross section. We can then conclude that, within the present experimental limitation, the overall global agreement here obtained between data and theory, assuming the present spectroscopic factor information, can be considered as a proof of principle of the analysis method.

VI. CONCLUSIONS

The heavy-ion reaction ^{48}Ca + ^{64}Ni, at few MeV per nucleon, has been investigated with the PRISMA-CLARA setup at LNL. The analysis focused on the study of the dynamics of the reaction, in particular of the elastic, inelastic, and one-nucleon transfer channels. Making use of particle-γ coincidences, angular distributions of the reaction products have been studied, also for particular excited states. A general agreement is obtained in the comparison with model predictions. Aside from the present limitations, the adopted analysis outlines a method which may provide additional, complementary information to more traditional analysis with light ions and sets the stage for future, systematic investigation of reaction mechanisms also employing radioactive heavy ions. In particular, higher sensitivity in the selection of specific excited states will be achieved, in the near future, by the combined use of magnetic spectrometers and advanced γ arrays, such as the European project AGATA [21,22]. This will result in very powerful setups which will allow to efficiently use γ-γ-particle coincidences to cleanly select excited states, making it possible to extract specific spectroscopic information. A first attempt of this kind of study is shown in Ref. [23].

ACKNOWLEDGMENTS

This work was supported by the Italian Istituto Nazionale di Fisica Nucleare and partially by the Spanish MICINN (ACI2009-1070 bilateral action) and Generalitat Valenciana (Grant Nos. BEST/2009/073 and PROMETEO/2010/101). The work has also been partially supported by the Polish Ministry of Science and Higher Education (Grant No. N N202 309135).

[1] D. R. Bes *et al.*, Phys. Rep. **34**, 1 (1977).
[2] R. A. Broglia and A. Winther, *Heavy Ion Reactions* (Addison-Wesley, Redwood City, CA, 1991).
[3] W. Reisdorf, J. Phys. G: Nucl. Part. Phys. **20**, 1297 (1994).
[4] L. Corradi, G. Pollarolo, and S. Szilner, J. Phys. G **36**, 113101 (2009).
[5] R. Broda, J. Phys. G: Nucl. Part. Phys. **32**, R151 (2006).
[6] J. J. Valiente-Dobon *et al.*, Phys. Rev. Lett. **102**, 242502 (2009).
[7] S. Bhattacharyya *et al.*, Phys. Rev. Lett. **101**, 032501 (2008).
[8] A. M. Stefanini *et al.*, Nucl. Phys. A **701**, 217c (2002).
[9] A. Gadea *et al.*, Eur. Phys. J. A **20**, 193 (2004).
[10] D. Montanari *et al.*, Phys. Lett. B **697**, 288 (2011).
[11] A. Winther, Nucl. Phys. A **594**, 203 (1995).
[12] M. Rhoades-Brown, M. H. Macfarlane, and S. C. Pieper, Phys. Rev. C **21**, 2417 (1980); **21**, 2436 (1980).
[13] G. Benzoni *et al.*, Eur. Phys. J. A **45**, 287 (2010).
[14] G. Montagnoli *et al.*, Nucl. Instrum. Methods Phys. Res. A **547**, 455 (2005).
[15] S. Beghini *et al.*, Nucl. Instrum. Methods Phys. Res. A **551**, 364 (2005).
[16] D. Montanari *et al.*, Eur. Phys. J. A **47**, 4 (2011).
[17] S. Szilner *et al.*, Phys. Rev. C **76**, 024604 (2007).
[18] L. Corradi *et al.*, Phys. Rev. C **66**, 024606 (2002).
[19] S. Szilner *et al.*, Phys. Rev. C **71**, 044610 (2005).
[20] National Nuclear Data Center, Brookhaven National Laboratory, [http://www.nndc.bnl.gov/].
[21] D. Bazzacco, Nucl. Phys. A **746**, 248c (2004).
[22] A. Gadea *et al.*, Nucl. Instrum. Methods Phys. Res. A **654**, 88 (2011).
[23] L. Corradi *et al.*, Phys. Rev. C **61**, 024609 (2000).